Control of a force-feedback teleoperated palpation device for minimally invasive thoracic surgery

Raquel Gacías

Master thesis submitted under the supervision of
Michel Kinnaert

The co-supervision of
Laurent Catoire

In order to be awarded the Master's Degree in
Industrial engineering (University of Zaragoza)

Academic year
2015-2016

Table of Contents

List of figures

List of tables

Abstract

Control of a force-feedback teleoperated palpation device for minimally invasive thoracic surgery. Master thesis written by Raquel Gacías as an Erasmus student during the academic year 2015-2016 to obtain the Master's Degree in Industrial Engineering by University of Zaragoza.

Key words: minimally invasive surgery, palpation, lung, force-feedback, teleoperation.

English

This work involves the developing of a teleoperated force-feedback palpation device in order to extend the possibilities of Minimally Invasive Surgery (MIS) in the thoracic field. Nowadays, detecting lung nodules during MIS has limitations because of the lack of direct contact, so they have to be located via the endoscope and a screen, which allows the surgeon to only detect visible nodules. In order to prevent this, a palpation teleoperation device was designed and built by Angelo Buttafuoco at the SAAS laboratory of ULB.

The robot is composed of a master device, manipulated by the surgeon, and a miniaturized slave device which is in contact with the lung and reproduces the task imposed by the master, and its purpose is to provide a haptic feeling to the operator for lung nodule detection during palpation through MIS.

This project aims at the implementation of adequate control laws between these two parts to allow restoring the operator's haptic sensation. In other words, permitting the surgeon to feel the lung as if he was actually touching it.

The design of the teleoperation control laws is carried out in MATLAB/Simulink and then implemented in the dSpace board via ControlDesk environment, all in communication with the device itself. Performance criteria had to be defined and experiments had to be designed in order to compare several controllers and to choose the most suitable one by testing and validating them first through simulation, and then by implementing them on the existing device. The palpation is performed on a mock-up reproducing a human lung.

French

Ce travail implique le développement d'un dispositif de palpation téléopérée afin d'étendre les possibilités de chirurgie mini-invasive (CMI) dans le domaine thoracique. Actuellement, la détection des nodules pulmonaires pendant la CMI a des limites en raison de l'absence de contact direct. Ils doivent donc être détectés par l'endoscope et affichés sur un écran, ce qui permet au chirurgien de détecter seulement les nodules visibles. Afin d'éviter

cela, un dispositif de palpation téléopéré a été conçu et construit par Angelo Buttafuoco au laboratoire SAAS de l'ULB.

Le robot se compose d'un dispositif maître, manipulé par le chirurgien, et un dispositif esclave miniaturisé qui est en contact avec le poumon et reproduit la tâche imposée par le maître. Son but est de fournir une sensation haptique à l'opérateur pour la détection des nodules pulmonaires pendant la palpation par CMI.

Ce projet vise à la mise en œuvre des lois de réglages adéquates entre ces deux parties pour permettre la restauration de la sensation haptique de l'opérateur. En d'autres termes, cela permet au chirurgien d'avoir des sensations similaires à celles qu'il retrouve lors d'une pratique classique.

La conception des lois de réglages pour la téléopération est effectuée avec MATLAB / Simulink et dans un environnement ControlDesk, tous en communication avec le dispositif lui-même. La réalisation de différents tests, validés d'abord par simulation, et ensuite par leur mise en œuvre sur le dispositif existant ont permis de comparer plusieurs régulateurs et de choisir le plus approprié. Pour ce faire, les critères de performance ont dû être définis et plusieurs expériences ont eu lieu. La palpation est effectuée sur une maquette reproduisant un poumon humain.

Dutch

Dees werk gaat over de ontwikkeling van een afstand bediende force-feedback palpatie apparaat om de mogelijkheden van Minimaal Invasieve Chirurgie (MIS) in de thoracale gebied uit te breiden. Tegenwoordig, vanwege het gebrek aan direct contact, heeft longknobbeltjes detectie tijdens MIS beperkingen. De longknobbeltjes moeten via een endoscoop en een scherm gevestigd zijn, daardoor kan de chirurg alleen toegankelijk knobbeltjes detecteren. Om dit te voorkomen, werd een palpatie teleoperatie apparaat ontworpen en gebouwd door Angelo Buttafuoco aan de SAAS laboratorium van de ULB.

De robot bestaat uit een masterapparaat, gemanipuleerd door de chirurg en een geminiaturiseerde slaveapparaat die in contact staat met de longen en reproduceert de taak opgelegd door de master. Het doel is om een haptische gevoel aan de operator te geven voor longknobbeltjes detectie via palpatie tijdens MIS.

Dit project richt zich op de implementatie van adequate control regels tussen deze twee delen om de haptische sensatie van de operator te herstellen. Met andere woorden, de longen voelen alsof daadwerkelijk contact bestaat.

Het ontwerp van de teleoperatie controle regels wordt in MATLAB / Simulink en in ControlDesk milieu uitgevoerd, allemaal in communicatie met het apparaat zelf. Prestatiecriteria moesten vastgesteld zijn en experimenten ontworpen om diverse controllers te kunnen vergelijken en de meest geschikte te kiezen. Om dit te doen, ondernemen we testen en validaties, eerst door simulatie, en vervolgens door de uitvoering op het bestaande apparaat. De palpatie wordt uitgevoerd op een mock-up dat een menselijke long reproduceert.

Acknowledges

I would like to express my gratitude to my promoter Michel KINNAERT for letting me join this project and guide me through it, and for his time flexibility.

Likewise, I would like to thank Laurent CATOIRE for his useful comments and his help introducing me to the technical details.

I need to thank Serge TORFS for his mechanical assistance and for making things work again when they didn’t.

I am also thankful for all the material from previous students that has been given to me to familiarize myself with the project.

And I could not forget to thank my family and friends, for whom distance has not been an obstacle for sending their love and support, and all the new friends that filled this year abroad with such amazing experiences.

Chapter 1

Introduction

1.1 Medical background

1.1.1 Minimally Invasive Surgery

Based on the degree of invasiveness of surgical procedures, we could define three main categories: invasive procedures (also known as open surgery), minimally invasive procedures and noninvasive procedures.

Minimally invasive surgery (MIS) provides great benefits to the patient over conventional open surgery such as reducing trauma, pain, blood loss and scarring, better cosmesis, less risk of complications and shorter recovery time for the patient [1].

However, MIS has also some disadvantages on the surgeon's performance due to the highly limited workspace and the reduced visual and touch information. Those are reasons why this kind of surgery requires special equipment and trained specialists. In order to minimize the MIS difficulties, we can find video-assisted and robot-assisted procedures [2].

Video-assisted surgery involves the insertion of a miniature camera through a small incision to allow the surgeon viewing and examining the patient. Additional specially designed instruments inserted through other incisions enable the surgeon to remove tissue.

Robot-assisted surgery also gives the surgeon access through small incisions, although in this case the specialist controls the robot's movements from the outside, with a master device in command of a slave one. Medical robots can incorporate sensors to return touch and force information, leading to an improved surgical performance. A worldwide example for carrying out this technique is the *da Vinci* surgical system, pictured in figure 1.1.

Figure 1.1: Master and slave devices of *Da Vinci* Surgical System [3]

1.1.2 Lung nodule detection, diagnosis and surgical intervention

A pulmonary nodule is a small round or oval-shaped growth in the lung, generally smaller than 3 centimeters in diameter [4]. There are two main types of pulmonary nodules: malignant (cancerous) and benign (noncancerous).

Usually there are no symptoms associated with pulmonary nodules, therefore most of the time a patient is unaware that he has a lung nodule until a chest X-ray or computed tomography scan of the lungs is performed.

Once a nodule is detected, it is necessary to determine the malignity of the lesion. If it is benign, it usually does not require treatment. However, if it is malignant, it should be surgically removed, and this step can be approached in different ways.

The less invasive option to take out a nodule would be a thoracoscopy where, as seen in figure 1.2, a flexible tube with a miniature camera allows the surgeon to view an image of the nodule on a screen, and the surgical instruments are inserted through the other incisions.

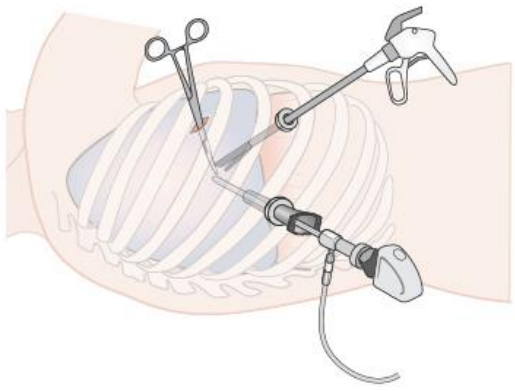

Figure 1.2: Diagram showing video assisted thoracoscopy [5]

This procedure is only feasible when the lesion is less than 3 cm away from a free edge of the lung, and when it is clearly visible. When these two requirements are not satisfied, it is needed to perform a thoracotomy, which is an open surgery where the surgeon palpates the lung, as in figure 1.3, looking for nodules so they can be removed, even if they are not visible.

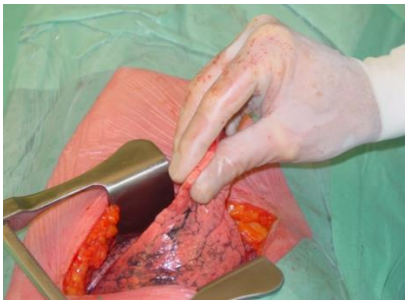

Figure 1.3: Palpation realized during thoracotomy [6]

Considering this information, MIS is the safest way to perform the ablation of peripheral pulmonary nodules, but its main problem is the lack of direct contact of the surgeon, so it is impossible to find invisible lesions.

Different ways of replacing or recreating the feeling of palpation for the surgeon can be found below in the next section.

1.2 State of the art

The mechanical devices adapted to MIS try to provide either tactile or kinesthetic feedback, but they are mainly experimental prototypes, as their miniaturization and sterilization are still a problem.

A first approach is providing visual information on the location of the nodules. An example of this would be a probe with a capacitive pressure sensor [7], which can detect pressure variations by pressing on a spot of the lung, and this information is available for the surgeon on a display.

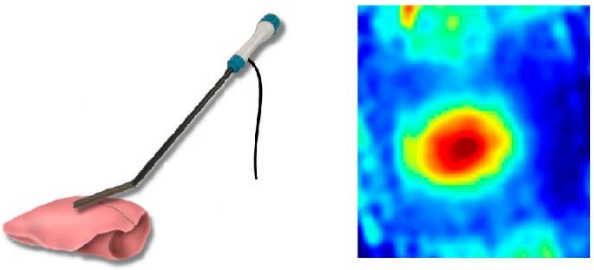

Figure 1.4: Capacitance-based sensor and pressure map

Another feasible possibility is an ultrasound probe [8] with a latex sleeve filled with ultrasound gel secured over the transducer, to improve contact between the transducer and the lung surface. 3D images are created by rotating the thoracoscopic ultrasound probe about its long axis while the transducer is maintained in close contact with the tissue.

Figure 1.5: Ultrasound-based sensor and 3D image

If we go one step further, we can introduce actual sensory feedback based on sensors transmitting information to actuators at the surgeon's fingers, with a control system in between, as seen in figure 1.6 [9]. This haptic information can be restored of both tactile and kinesthetic information. Tactile information is useful in providing touch sensation to the user, while kinesthetic feedback provides a sense of position and movement of the robotic end-effectors relative to tissues in the body.

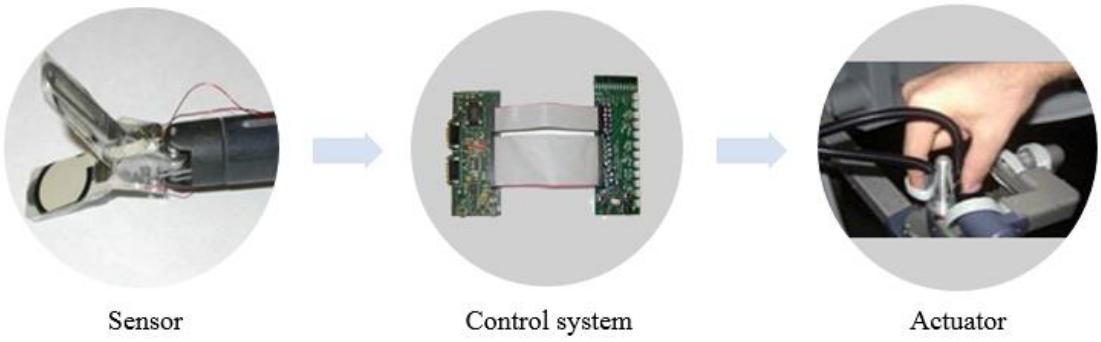

Figure 1.6: Haptic feedback system concept

Several options for sensing can be found, such as capacitive sensors, magnetic coil sensors, magnetoelastic sensors, optical sensors, piezoelectric sensors, piezoresistive sensors, strain gauges, spring-loaded whisker sensors and ultrasonic sensors. In the same way, there are different means to provide sensory feedback, including motor driven

actuation, vibrotactile displays, piezoelectric actuators, shape memory alloys, rheological fluids, and pneumatically driven actuators [9].

As explained above, haptic information can be divided into two categories: kinesthetic and tactile. Kinesthetic information relates to the movement and bulk forces acting in the joints of the arm, if any, and at the point of contact. The contour and stiffness of an object can be determined through kinesthetic information via a force/torque sensor. In contrast to kinesthetic information, tactile information includes the sensation of surface textures, or distributed pressures acting across the contacting surface, being able to potentially collect more information than kinesthetic feedback while palpating tissue. However, it is more complicated since it often requires an array of sensing elements to determine pressures over a small area [10], incurring higher costs because of the technology employed.

Since the final goal, expounded in the next section, is to distinguish hard nodules from healthy soft tissues, the kinesthetic approach fits for purpose.

1.3 Aim of the project

The work in this project is based and tested on a master/slave device for teleoperation designed by A. Buttafuoco [6], and it takes as starting point the need to continue the previous studies on the existing device, whose objective is to make nodule palpation practicable without renouncing to the advantages of MIS.

The first steps required a wide medical study regarding lung anatomy, pulmonary nodule diagnosis and different procedures for addressing the surgery. This stage counted on the help of thoracic surgeons on the basis of the study of the medical gesture.

The conclusions of those researches led to the designing step, which included the choice of suitable architectures, materials and instrumentation. The mechanical design, presented in figure 1.7, will be explained with more detail in Chapter 2.

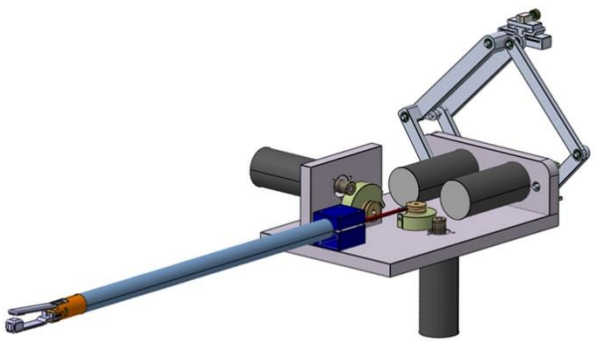

Figure 1.7: CAD design of the teleoperation device [6]

Once the device was fully assembled it was necessary to control it, so a model of the whole system was made in order to carry out theoretical studies on its teleoperation, including the model of the human operator, the model of the lung and the models of the master and slave devices. Three different alternatives of control schemes were studied and simulated, such as a Position-Position scheme, where only position measurements are exploited to implement the force feedback, a Force-Position scheme that also requires a force sensor at the slave side, and a 3-Channel control scheme which needs force sensors at both ends of the device [6].

In addition to Buttafuoco's work, there were some other projects more focused on specific matters, such as the implementation of the position-position control scheme for teleoperation [11] and the control of the compression arm of the slave [12].

The current work covers different steps in order to have the complete master-slave system operational by the end of the project. Those steps include the control of the shear arm of the slave, the introduction of a force-feedback control on the system and, in the end, grouping the different studies for developing and implementing the teleoperation control laws for the palpation task.

Chapter 2

Specifications

2.1 Architecture of the palpation device

2.1.1 Overview

The device can be divided in two main mechanical structures: a pantograph-like master and a slave grasper designed to have two degrees of freedom. The assembly of those parts is done as in figure 2.1.

The master part is manipulated by the surgeon. Due to the human-master interaction, several criteria such as ergonomics, low weight and low inertia had to be taken into account during the design process.

The slave has to perform the palpation task, so it needs to enter a small trocar, for which the size of this part was also an important parameter to minimize, without neglecting the importance of the weight, the inertia and the friction.

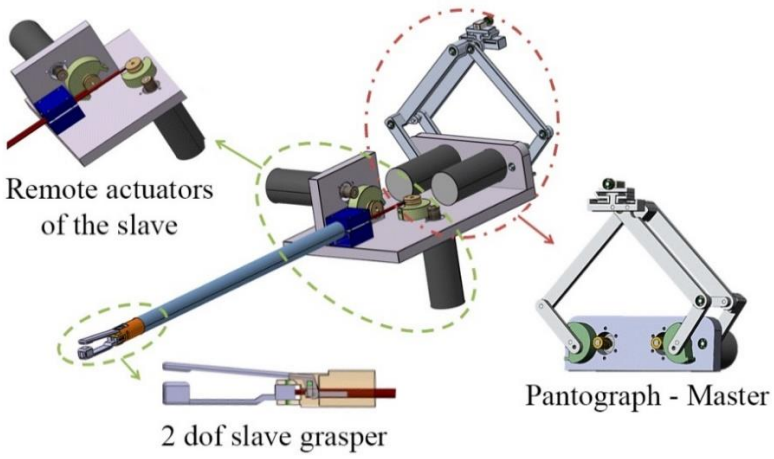

Figure 2.1: Assembly of the palpation device

To allow the interaction between the operator and the environment, both parts of the device are equipped with sensors and actuators so that there is a flow of information in both ways. The sensors and the basic structure of the master and the slave are detailed below. Also, both at the slave and at the master side, capstans are used to increase the available torque.

2.1.2 Master device

The operator of the device supports the master with one hand and manipulates it with the other thanks to the handle at the top of the device (figure 2.2). The only desired movements to be performed are horizontal and vertical displacements, so a pair of passive moving arms is added to the device so it has a parallelogram-like structure that imposes the orientation of the sensor, allowing it only to translate.

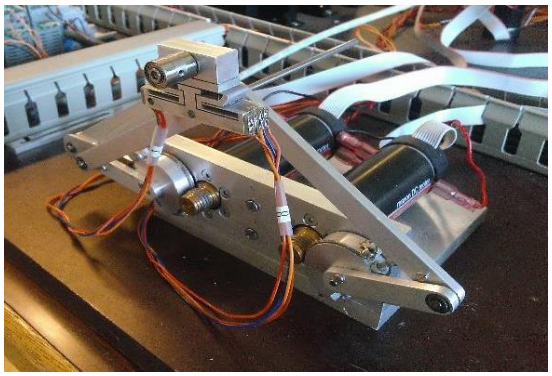

Figure 2.2: Picture of the master device

The arms of the pantograph are moved thanks to a pair of DC motors on the base of the master, with enough nominal torque to perform as expected but with a low mass.

The force sensor, located on top of the master, is a flexible body made of aluminum with a sensing circuit integrated on it, composed by strain gauges. These gauges are placed in such a way that the sensor can measure both lateral and vertical forces, depending on if the springs of the body are deformed in the same direction or in opposite directions (figure 2.3).

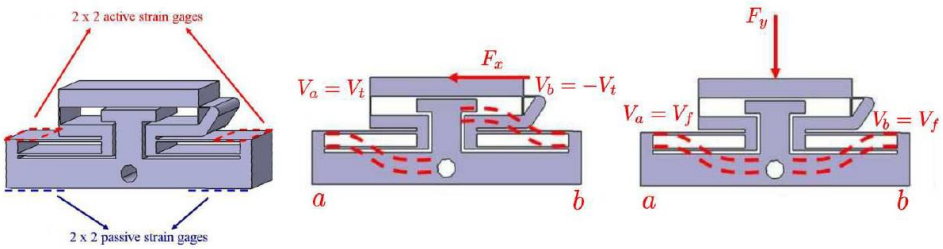

Figure 2.3: Force sensor and its deformation when applying forces

2.1.3 Slave device

The grasper of the slave (fig. 2.4) is composed of two moving arms, the upper one acting in compression while the lower one in shear. Unlike the master device, which is manually moved by an operator, the slave's movements are commanded by the first one, so its upper arm will move according to the vertical displacements of the master and the lower one will do it with the horizontal motion.

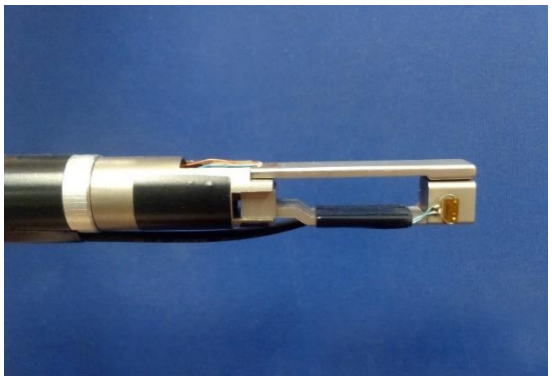

Figure 2.4: Picture of the grasper on the slave device

The actuators are again DC motors, but in this case they must be in a remote place due to the need of the slave to be inserted in the patient's body. The motion transmission between the actuators and the arms is carried out by pulleys and rods, and the assembly can be seen in figure 2.5.

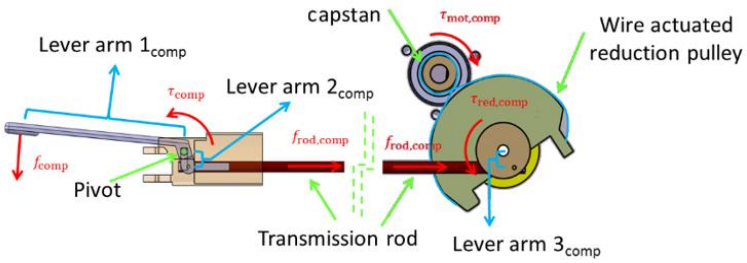

(a)

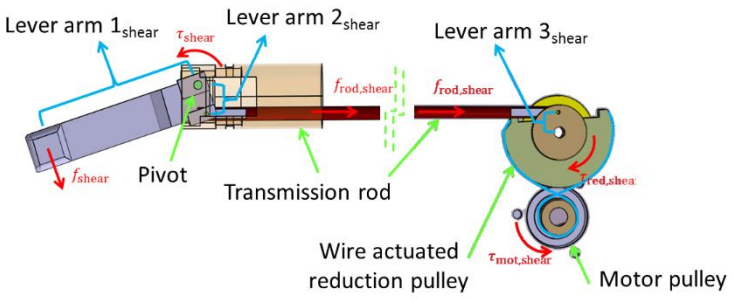

(b)

Figure 2.5: Elements of the slave device: (a) Compression arm; (b) Shear arm

Force is also measured here by strain gauges, placed in both arms. The compression arm has the strain gauge directly attached to itself, while for the shear arm there is a force sensor (fig. 2.6) which acts as the support for the strain gauges, as seen on the assembly on figure 2.4.

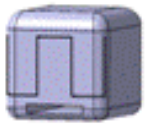

Figure 2.6: Shear force sensor

2.2 Components

The desired performance of the device is feasible thanks to a set of external items that allow the system to move properly, to sense the environment and to be controlled. All these components were chosen as a result of the previously mentioned studies done by Angelo Buttafuoco.

As commented before, both the master and the slave have actuators for their motion, MAXON RE25 motors [13] with encoders to measure their position and current controllers from the same manufacturer for driving them (ADS 50/5 and ADS 50/10).

The strain gauges that are used for measuring correspond to the Vishay PB60 model [14], and they are self-temperature-compensated gauges to avoid problems due to thermal effects. Their outputs are amplified thanks to amplifiers with a 500 Hz bandwidth.

The communication between the palpation device and the user interface comes from a DS1103 PPC Controller Board from dSpace [15].

2.3 System operation

The programming of the system is done in the Simulink environment of MATLAB [16], and it interacts with ControlDesk [17], which is the software of the dSpace board where the user can visualize the inputs and outputs of the system and act on them. The board sends the pertinent signals to the current controllers and these latter feed the different motors. Appendix I collects the main features of this software.

The signals in and out of the board go through different channels. The table below collects the information on what is connected to each channel.

Channel	Signal
Input 3	Left encoder of the master
Input 5	Right encoder of the master
Input 6	Encoder on the shear arm of the slave
Input 7	Encoder on the compression arm of the slave
Output 3	Right motor of the master
Output 4	Left motor of the master
Output 5	Motor on the compression arm of the slave
Output 6	Motor on the shear arm of the slave

Table 2.1: Space board channel connections

Chapter 3

Motion control of the device

3.1 Modelling

3.1.1 Method

The goal of this chapter is to obtain a model of the behavior of the two arms that the grasper is composed of. The input of the system is a current reference and the output is the position of the arm expressed in degrees, and the procedure consists on retrieving the parameters of the system by taking and analyzing a series of measurements. Motion control is done here without interaction with the environment.

The generic model is based on a simple model for the dynamics of a manipulator, where there are no forces acting on the end-effector:

$$B(\theta)\,\ddot{\theta}(t) + F\left(\theta, \dot{\theta}\right)\dot{\theta}(t) + g(\theta) = \tau_m(t)$$

where $\tau_m(t)$ is the total torque applied to the system, $B(\theta)$ is the inertia matrix, $F\left(\theta, \dot{\theta}\right)$ represents the friction effects and $g(\theta)$ is the vector of gravity forces, which can be neglected for this case, as stated on previous works [11].

By defining $B = \tau \,/\, K$ and $C = 1/K$, being τ the time constant of the system and and K its gain, and removing the gravity term, the equation can be rewritten as:

$$\frac{\tau}{K}\,\ddot{\theta}(t) + \frac{1}{K}\,\dot{\theta} = \tau_m(t)$$

The Laplace transform is applied and the terms are reorganized, resulting in the following equations:

$$\frac{\tau}{K}\,\Theta \cdot s^2 + \frac{1}{K}\Theta\, s = T_m$$

$$M(s) = \frac{\Theta}{T_m} = \frac{\mathrm{K}}{\mathrm{s} \cdot (\tau \mathrm{s} + 1)}$$

The obtained model is a second order system, where one of its poles is at the origin. Due to these dynamics, the proposed input is a pulse, but in order to avoid static friction effects, the input is applied when the corresponding arm is already moving, so a step is previously used.

The pulse is employed when the arm reaches a certain angle, and this angle will be varied on each measurement in an attempt to cover a wider range. The magnitude of both the step and the pulse can also change depending on the moment where the pulse is applied.

These inputs and the response of the system will be described with more detail on section 3.1.3.

3.1.2 Characterization of the starting current

It is important to know the value of the minimal current that is required for an arm to move because of friction effects. That is achieved by applying a current ramp with a low slope to the system and measuring when the arm starts to move.

This method is used on both arms and on each direction that an arm can move. The results allow to set a minimum level of friction that the system needs to overcome.

Figure 3.1 represents the position of the shear arm when applying a ramp as an input, and the moment when the position starts to defer from zero is where the value of the minimum current needed is obtained.

Those input values are directly the ones applied to the actuators, in DSP units, but they can easily be converted into a current value or a torque value with the known gains of these motors, which are:

$$G = 10\ [\,{}^{V}/_{DSP}\,]$$

$$G_I\ (ADS\ 50/5) = 0.5\ [\,{}^{A}/_{V}\,] \qquad G_I\ (ADS\ 50/10) = 1\ [\,{}^{A}/_{V}\,]$$

$$K_c = 0.02532\ [\,{}^{Nm}/_{A}\,]$$

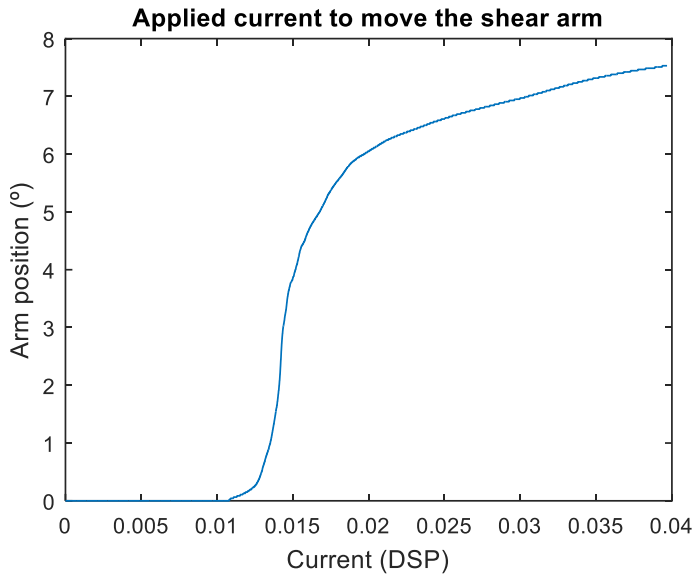

Figure 3.1: Behavior of the shear arm when the input is a ramp

After carrying out a number of measurements, the average value of the current that is needed for the grasper to start moving are the ones on table 3.1.

Case	Mean (DSP)	St. dev. (DSP)
Shear arm moving towards left	0,0111	0,0079
Shear arm moving towards right	0,0268	0,0047
Compression arm opening	0,0112	0,0032
Compression arm closing	0,0122	0,0027

Table 3.1: Starting current average values

These values will be useful to characterize the minimum friction for the simulation in the following sections, and they show that the friction for the shear arm is not only more unbalanced between the two directions but has also a higher variability.

3.1.3 Response of the system

Once the measurements have been made, the data is collected in MATLAB in order to be treated and save the interesting parts of each sample. Figure 3.2 shows the whole response of one of the arms and the corresponding input (amplified by 50). The arm starts moving when the step is applied and there is a change in the slope after the pulse due to the fact that the friction is not constant, and the arm keeps moving until it reaches its mechanical limit.

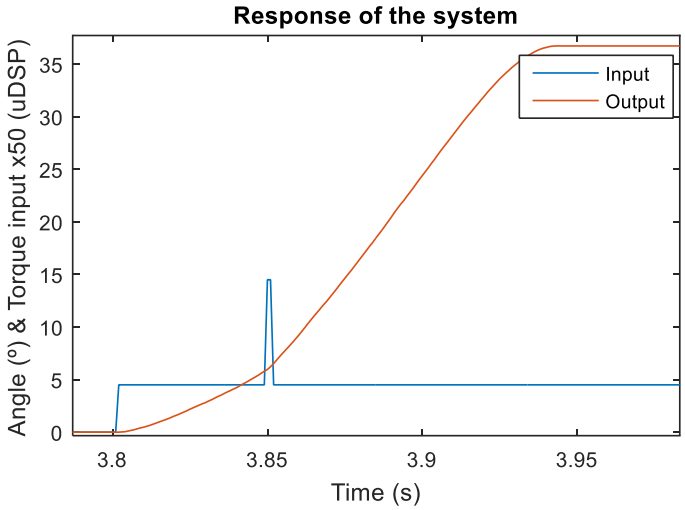

Figure 3.2: Response of the shear arm with an impulse at 5º while moving

To find the best model, the measured trajectory will be limited to tens of milliseconds after the pulse is applied. As mentioned previously, the magnitudes of pulse and step are tweaked each time so that it is neither too weak (where the arm wouldn't move) nor too strong (where it would reach too fast the end of its range of motion). The amount of data treated after the pulse will also change according to the angle of impulsion, decreasing when the angle increases, due to the fact that the mechanical end of the arm is closer.

3.1.4 Optimization of a model

The procedure of finding the fit of a model starts with an estimation of two parameters: the gain and the time constant of the model. These estimations, whose value is not very influential on the results, are used to simulate a response with the same input as the real measurements, and the given results are compared with the real ones with the least-square method. Thus, both parameters are optimized by minimizing the error between the response with the estimated system and the real one.

First, a step is applied in a fixed time, and then there is a pulse generator that is only employed when the angle of the arm reaches an imposed threshold.

There are also some protection measures, as a saturation of the input to avoid high values that could damage the system, or a stop command where the angle reaches the limit of the arm's range of motion, to prevent applying torque when the arm can't physically move.

The tables below collect the obtained parameters for each measurement and the characteristics of the data treatment for each arm and each direction of motion. Those parameters are the amplitude of the step and the pulse, the width of the data window used for the optimization (duration of fit) and the time constant and gain of the optimized model, where that model has the same structure in all cases, the one obtained in section 3.1.1.

Angle of impulsion (º)	Step amplitude (uDSP)	Pulse amplitude (uDSP)	K	τ (s)	Duration of fit (ms)
20	0,017	0,03	3832	0,08275	250
25	0,017	0,03	8658	0,08163	80
30	0,017	0,03	5900	0,01428	60
35	0,017	0,03	4199	0,05384	30

Table 3.2: Parameters for the compression arm while closing

Angle of impulsion (º)	Step amplitude (uDSP)	Pulse amplitude (uDSP)	K	τ (s)	Duration of fit (ms)
20	0,02	0,085	9607	0,00316	20
30	0,018	0,07	5598	0,006239	20

Table 3.3: Parameters for the compression arm while opening

Angle of impulsion (º)	Step amplitude (uDSP)	Pulse amplitude (uDSP)	K	τ (s)	Duration of fit (ms)
3	0,09	0,15	2040	0,008505	100
5	0,09	0,2	4360	0,02600	80
10	0,09	0,2	4813	0,02089	60
15	0,09	0,2	5033	0,01521	50
20	0,09	0,2	4339	0,005072	30

Table 3.4: Parameters for the shear arm while moving towards right

Angle of impulsion (º)	Step amplitude (uDSP)	Pulse amplitude (uDSP)	K	τ (s)	Duration of fit (ms)
2	0,09	0,15	2110	0,01036	30
3	0,09	0,15	1833	0,01001	20
5	0,1	0,1	2576	0,01249	30
10	0,1	0,15	2535	0,01192	30
15	0,1	0,15	3002	0,009168	30

Table 3.5: Parameters for the shear arm while moving towards left

The retrieved parameters of the different models vary across the range of motion because the system does not behave the exact same way, but that variation will be compensated with the use of a disturbance observer.

Figure 3.3 shows the fit of one of the models to the real data, simulated with the *lsim* MATLAB command, being this case the one where the pulse is applied at 5º when the shear arm is moving towards right. The real output remains very close to the simulation until it reaches the mechanical limit of its range of motion, where it stops.

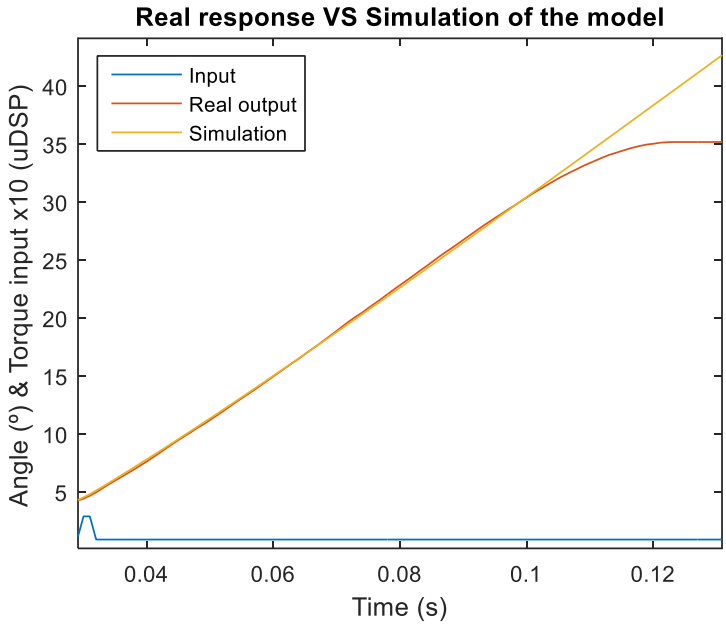

Figure 3.3: Real output and simulation of the obtained model for the same input

3.2 Position control

Position control (fig. 3.4) is made with a PD controller, whose characteristics are chosen over one model, and then simulations with the rest of them will be done to check if the behavior is appropriate.

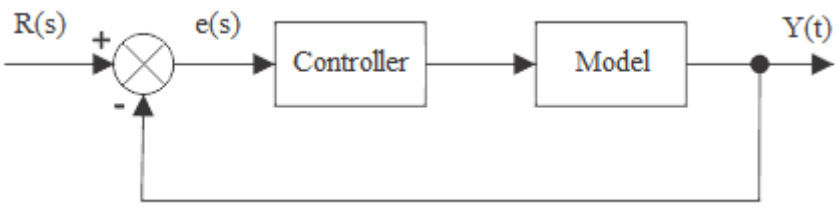

Figure 3.4: Block diagram for position control

The controller is composed of a gain, one zero and one pole:

$$C\ (s) = Kp \cdot \frac{\tau 1 \cdot \mathrm{s} + 1}{\tau 2 \cdot \mathrm{s} + 1}$$

The zero is chosen so that it cancels the non-zero pole of the model, the controller's pole will be five times faster than its zero, and the gain will have the value that gets a damping factor of 0.7 for the system.

The root locus for the model and the controller without the gain is the one in figure 3.5. Matlab function *zgrid* generates a grid of constant damping factors as in figure 3.6, and function *rlocfind* allows to find the value of the gain for the intersection point between the root locus and the line of the desired dampling factor.

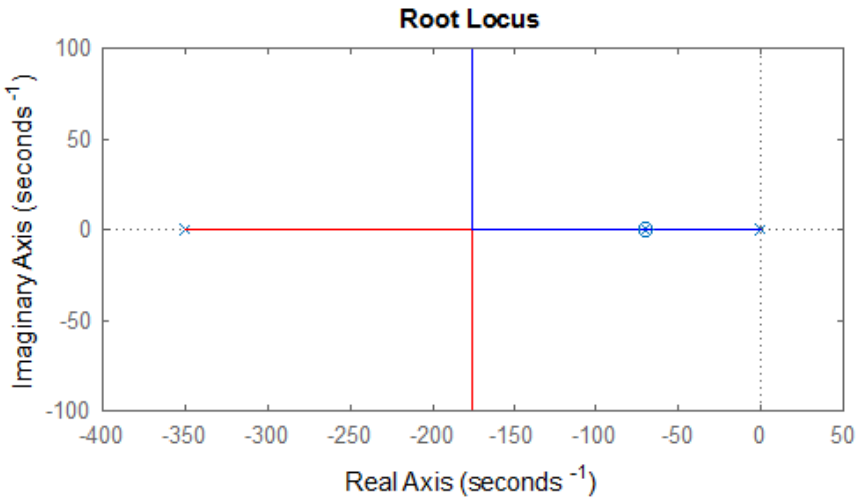

Figure 3.5: Root locus of the system

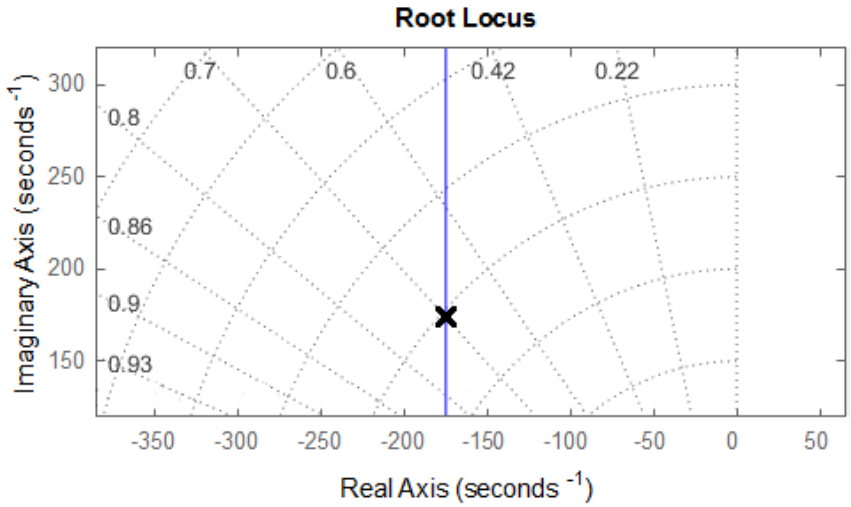

Figure 3.6: Root locus with the interesting point to obtain the gain

Taking into account these considerations, the controllers for the shear arm and the compression arm are calculated and presented in table 3.6. They have been determined according to the chosen models on the same table, whose choice is based on common angles of the grasper during palpation.

Arm	Chosen model	Controller
Shear	$\frac{2535}{s \cdot (0.01192 \cdot s + 1)}$	$0.0819 \cdot \frac{0.01192 \cdot s + 1}{0.002384 \cdot s + 1}$
Compression	$\frac{5900}{s \cdot (0.01428 \cdot s + 1)}$	$0.0295 \cdot \frac{0.01428 \cdot s + 1}{0.02856 \cdot s + 1}$

Table 3.6: Chosen model and controller for both arms of the grasper

Stability of the system has been checked by obtaining the gain and phase margins for all the models of tables 3.2 to 3.5, in an open loop with the controller, where all of them have gain margins above 6 dB and phase margins higher than 45º.

3.3 Simulation

Now that the system is modelled and the controller designed, the next step is validation through simulation and seeing if the behavior is the expected one in order to be able to implement it. Once again, that is carried out via Simulink according to the schematic in figure 3.7 and it is going to be done with and without a disturbance observer to see its influence.

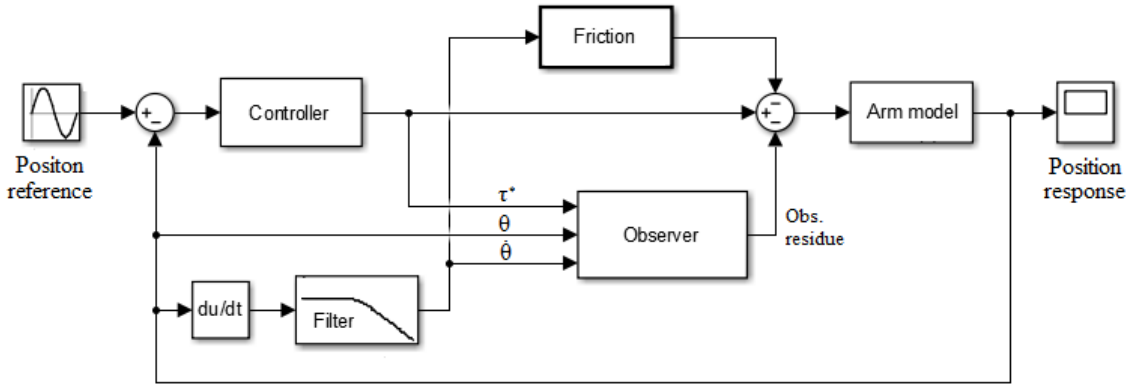

Figure 3.7: Schematic for simulation of motion control of one arm

This observer (fig 3.8) is based on the system of section 3.1.1 with the parameters of the chosen model on 3.2 and acts directly on the command applied to compensate it when the system deviates from the model, using as input the position, the velocity and the torque.

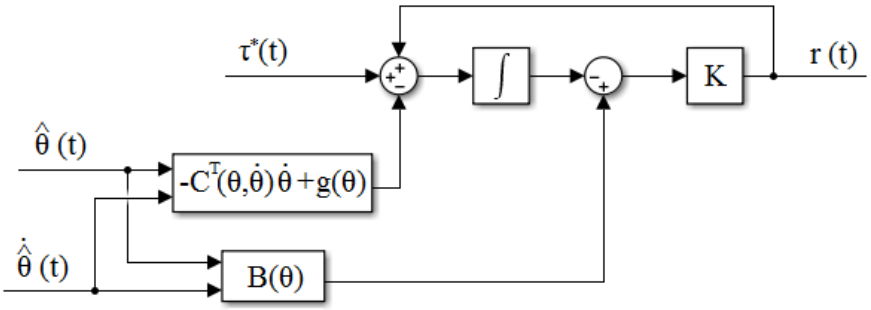

Figure 3.8: Schematic for the disturbance observer

For the velocity signal, the only available measure is the position provided by the encoders, so it needs to be derivated. Due to the quantization of the encoders, the signal after derivation is filtered with a second order low-pass Butterworth filter, which has a 30Hz bandwidth.

The selected input is a non-centered sine wave with a 4 rad/s frequency and an amplitude of 10º in an attempt to present a motion that is similar to the one that the operator does during palpation. There is also Coulomb friction model added to the system to include in the simulation the friction that was measured in section 3.1.2.

The simulation has been done for both arms, and the results for the lag and error can be found below on table 3.7.

Compression arm	**Lag (ms)**	**Error (%)**
Without observer	7	0,9
With observer	1,4	0,1

Shear arm	**Lag (ms)**	**Error (%)**
Without observer	13	1,55
With observer	5	0,35

Table 3.7: Numerical simulation results

These values prove that both the lag and the error are smaller when the observer is included on the scheme, and that the performance of the compression arm is better, as expected from the obtained friction values.

3.4 Implementation

The implementation on the device is based on the same block diagram, except that now it is necessary to remove the model of the system and introduce the parts corresponding to the real system, namely the encoders of the controlled motors for the position sensor, and the actuators that the commands are sent to. Also, as in all schemes to be implemented on the real device, saturation blocks are used for protection. The complete block diagram of this implementation, as well as the rest of Simulink schematics, can be found in appendix II.

Figure 3.9 shows the response of each arm when a sine input is applied. For the compression arm, the real lag is 1.25 ms and the error between the reference and the response is 0.16 %. These values are consistent with the ones obtained in simulation. The shear arm has a lag of 6.7 ms and an error of 1.4 %, which is a behavior a little bit worse than the expected one, difference that can be explained with the friction on that arm being more difficult to model because it depends on the position of the arm.

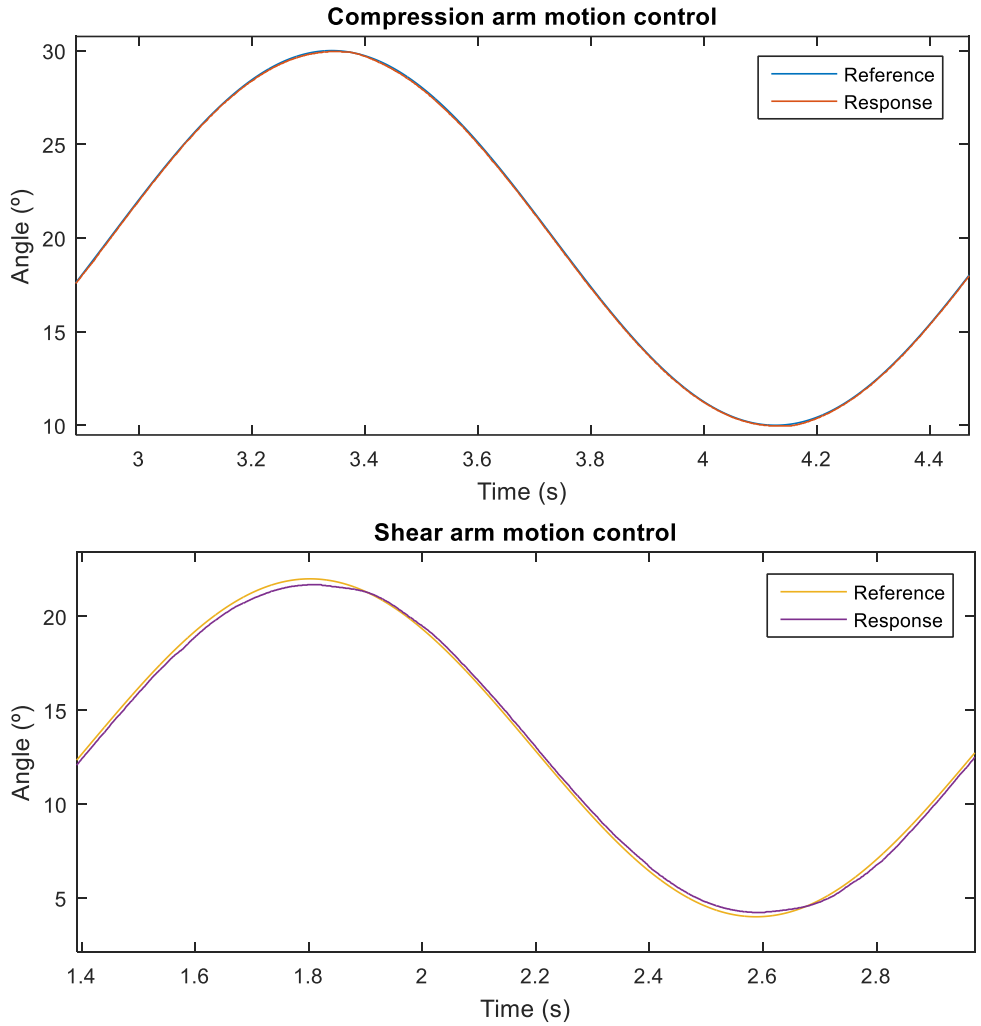

Figure 3.9: Implementation results for both arms

3.5 Conclusion

The slave device has been modeled and a controller has been designed, simulated and tested in implementation in order to control its motion. The obtained results, whilst they are not perfect, reach the expectations, because both the lag and error are small enough for palpation purposes.

The next step is to use these controllers to put the device in teleoperation by using the motion of the master as a reference to the slave, which is the purpose of next chapter, along with the incorporation of the force-feedback.

Chapter 4

Teleoperation

4.1 Unilateral teleoperation

4.1.1 Analysis and implementation

This first part of the chapter introduces a one-way teleoperation, where the position of the master serves as a reference for the control of the slave (fig.4.1).

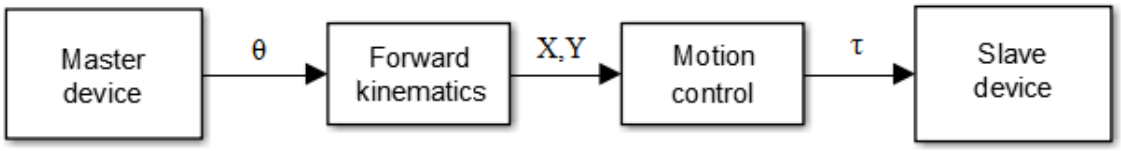

Figure 4.1: Unilateral teleoperation flow chart

The motion of the master is generated by hand, and the goal is that vertical movements are transferred to the slave as a motion on the compression arm and horizontal movements become a motion of the shear arm.

This implementation needs the forward kinematics of the pantograph of the master described on [6], with the following equations based on the pantograph scheme on figure 4.2:

$$P_3 = \begin{pmatrix} l_1 cos\theta_{m,1} \\ l_1 sin\theta_{m,1} \end{pmatrix} \qquad P_4 = \begin{pmatrix} d + l_2 cos\theta_{m,2} \\ l_2 sin\theta_{m,2} \end{pmatrix}$$

$$\|\overline{P_3 P_H}\| = \frac{l_3^2 + \|\overline{P_3 P_4}\|^2 - l_4^2}{2 \cdot \|\overline{P_3 P_4}\|}$$

$$P_H = P_3 + \|\overline{P_3P_H}\| \frac{(P_4 - P_3)}{\|\overline{P_3P_4}\|}$$

$$\|\overline{P_HP_M}\| = \sqrt{l_3^2 - \|\overline{P_3P_H}\|^2}$$

$$P_M = P_H + \|\overline{P_HP_M}\| \begin{pmatrix} 0 & 1 \\ -1 & 0 \end{pmatrix} \frac{(P_4 - P_3)}{\|\overline{P_3P_4}\|}$$

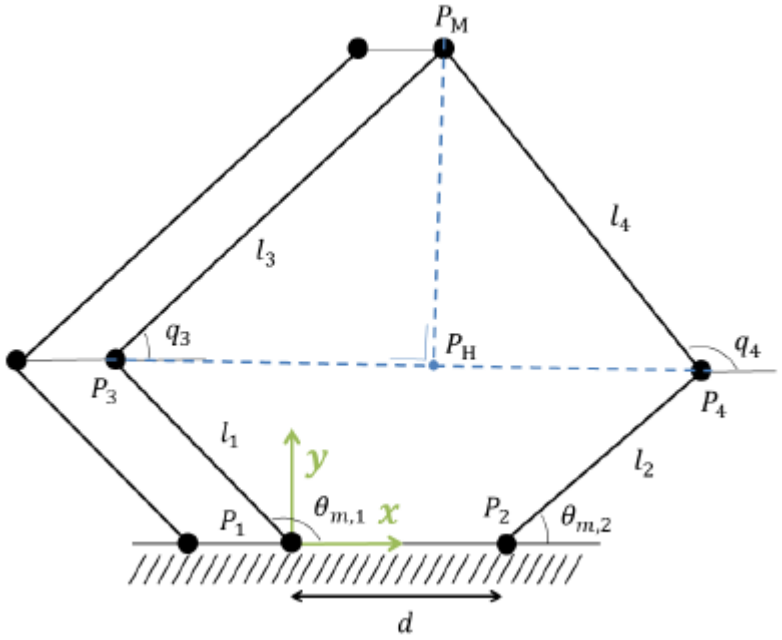

Figure 4.2: Scheme of the pantograph

This way, the Cartesian coordinates of the tip of the master (in meters) are computed from the angles given by the encoders of the motors (in radians).

For the interaction of the master device and the slave device, there needs to be some adaptation in terms of magnitudes, where the position of the master after the forward kinematics is expressed on a xy-plane and the slave position is described with angles.

The master tip is physically constrained by a 30x30 mm square-shaped guide, and the slave limits are set as [0º,+40º] for the compression arm and [-20º,+20º] for the shear one. Measurements have been made within that space to obtain the necessary equations to relate the position of the master and the slave (table 4.1), and also to know the values of the real limits in order to set them as a saturation limit later on the implementation.

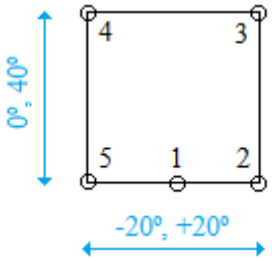

Point	Master coordinates (x,y) [m]		Slave angles (shear, comp) [º]	
1	0,0884	-0,00925	0	0
2	0,0778	-0,01071	20	0
3	0,0703	-0,04281	20	40
4	0,08905	-0,04926	-20	40
5	0,0943	-0,01132	-20	0
6	0,08864	-0,009142	0	0

Table 4.1: Motion space limits

With those measurements, the conversion between the x and y coordinates into angles is done by the following straight-line equations:

$$Shear\ angle\ [º] = -1980{,}2\ [º/m] \cdot x_M\ [m] + 165{,}1485\ [º]$$

$$Compression\ angle\ [º] = -1078{,}2\ [º/m] \cdot y_M\ [m] + 90{,}027 [º]$$

where x_M and y_M represent the position of the tip by the master, obtained from the encoders of its motors and the direct kinematics of the pantograph.

All the mentioned conversions are implemented as in figure 4.3, along with the gain of the encoders (to convert pulses to radians) and the reduction of the capstan.

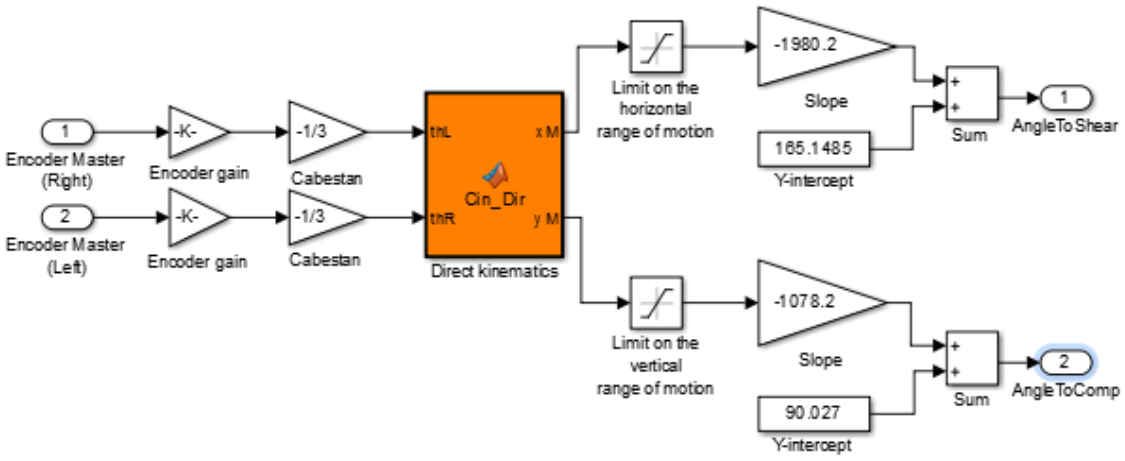

Figure 4.3: Adaptation of the reference for the slave

The output values of the last scheme, *AngleToShear* and *AngleToComp*, are the references for the motion control of both arms of the slave, as it was implemented on the previous chapter.

4.1.2 Results

Once the device is connected, the operator moves the master device freely in the allowed space, which brings simultaneous motion of both of the arms of the slave. Figure 4.4 shows the performance of this unilateral teleoperation, where again the behavior of the compression arm is better with a ~3 ms lag against a ~14 ms lag on the shear arm.

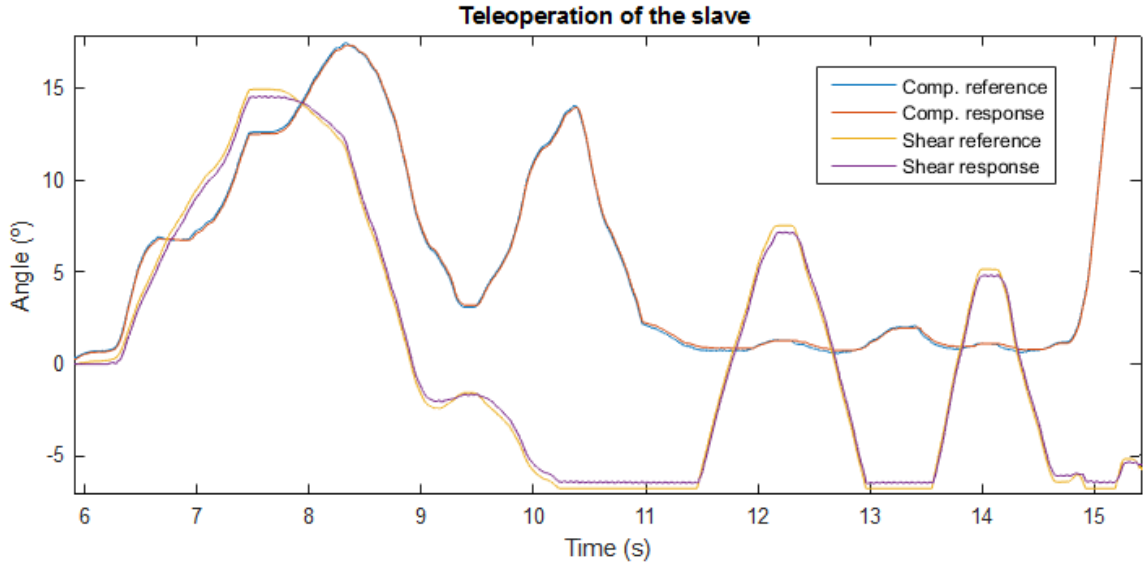

Figure 4.4: Response of the slave with the position of the master as an input

This first test is carried out without any interaction between the environment and the slave, but the main purpose of the grasper is to have that interaction, where forces are generated between the arms of the slave and the surface in contact.

By measuring those forces, a haptic feeling can be provided to the operator. This will result in a bilateral teleoperation, which is explored on the next section. Bilateral teleoperation can also be achieved with different approaches, as it was done in [11] with a position-position control scheme, where the position of the master serves as a reference for the slave (as in this chapter) but also the position of the slave becomes a reference for the motion of the maser.

4.2 Bilateral teleoperation

4.2.1 Force-feedback inclusion

In order to retrieve a haptic feedback to the master, the force sensors of the slave that were designed on Buttafuocco's work are employed. Regarding the compression force, there are two strain gauges directly fixed at the basis of the upper arm, whereas for

the shear force there is a specifically designed deformation body with strain gauges bonded on its sides.

The force sensors were calibrated in previous works in order to find the equations that characterize them, but they have been found not to be very precise anymore due to changes on the device over time. However, the main goal here is to detect a difference between the force when there is no nodule on the lung and the force when there is, and that can be achieved even if the real values of the force are unknown. For that purpose, the measurements have been processed and adapted in order to have adequate output values.

The output of each force sensor has been measured in a steady state to have their offset values, which are gathered in table 4.2.

Sensor	Offset value (V)
Master left	-0,67
Master right	-0,28
Slave comp.	-0,835
Slave shear (b)	-0,009
Slave shear (o)	-0,012

Table 4.2: Offsets of the force sensors

As a start to test the behavior of the sensors when there is a constraint in the movement of the slave, an obstacle has been placed within its range of motion. The response of the compression arm (still in unilateral teleoperation) is in fig. 4.5, where the reference is not reached whenever the obstacle interferes, and that generates a compression force, which is the one that is wanted to be transferred to the master.

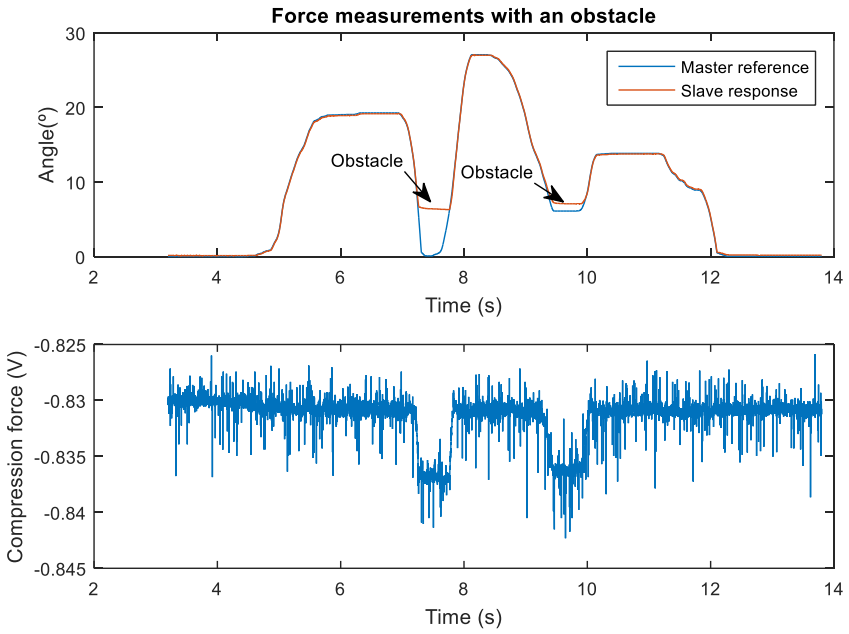

Figure 4.5: Response of the slave with an obstacle and the pertinent force signal

It can be seen that the signal coming from the force sensor is very noisy, so it needs to be filtered in order to prevent vibrations on the actuators, which is an undesirable behavior for any device, but especially for a surgical one.

For the filtering, a 2nd order low-pass Butterworth filter is chosen and included on the schematic. The data is acquired in real-time at a 10 kHz frequency and the chosen cutoff frequency is 50 Hz, so the normalized frequency of the filter is 0.01π rad/sample. The comparison of the original and the filtered signal is shown on figure 4.6.

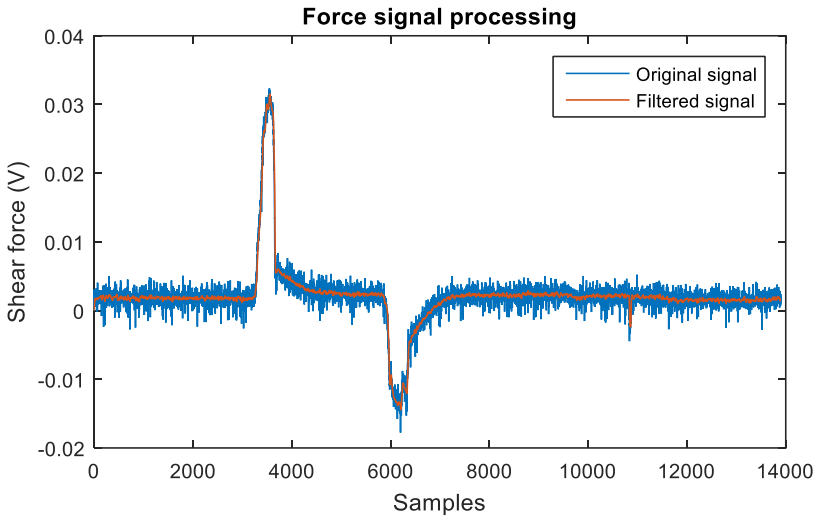

Figure 4.6: Filtering of a signal from a shear force sensor

Once the force sensors are operative, testing is made with the mock-up lung shown in figure 4.7 to measure the response of the sensors during palpation. This representation of a lung is composed of a solution made out of polyvinyl alcohol, sodium tetraborate and distilled water, and it has some little latex balls simulating the lung nodules.

Figure 4.7: Mock-up lung for palpation tests

4.2.2 Analysis and implementation

The first attempt for the bilateral teleoperation is done as in figure 4.8. The force control is done with an open-loop controller, where the torques to be send to the actuators of the master are calculated with the Jacobian of the pantograph and the measured forces in the slave.

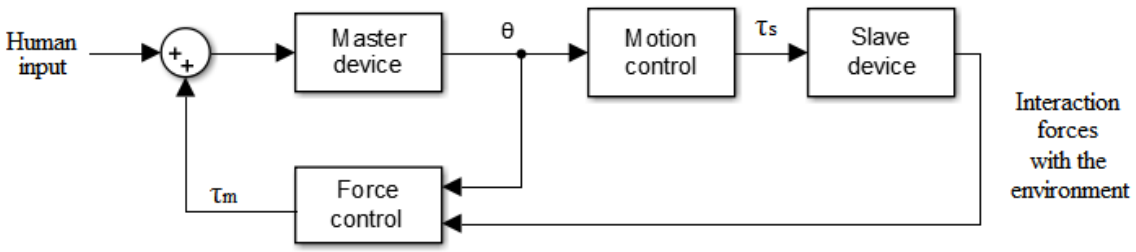

Figure 4.8: Bilateral teleoperation flow chart

Figure 4.9 represents how the force control is done in control loop (the complete Simulink schematic can be found on appendix II). The forces measured by the slave force sensors, F_x and F_y are pre-multiplied by the transposed Jacobian matrix of the pantograph in order to obtain the needed torques at the actuators of the master for having those forces at its end.

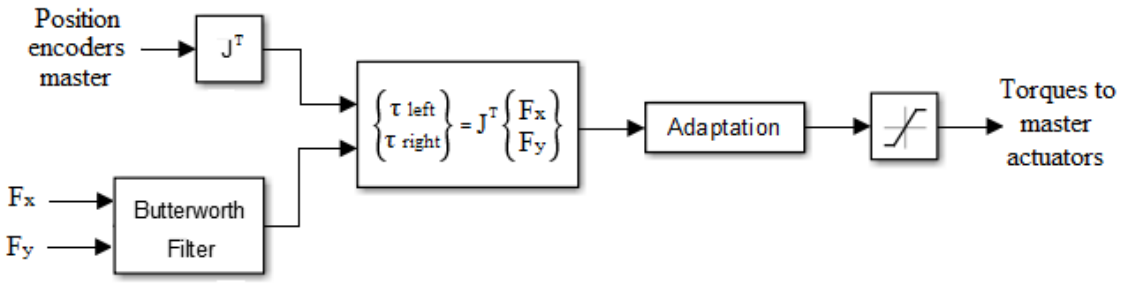

Figure 4.9: Force control schematic

The Jacobian matrix is defined as:

$$J = \begin{bmatrix} \frac{\partial x_M}{\partial \theta_{left}} & \frac{\partial x_M}{\partial \theta_{right}} \\ \frac{\partial y_M}{\partial \theta_{left}} & \frac{\partial y_M}{\partial \theta_{right}} \end{bmatrix}$$

where x_M and y_M are again the coordinates of the tip of the master and θ_{left} and θ_{right} are the angular position of the left and right motors of the master.

For the adaptation part, there was the need of a range of adequate torque values for this application, and by testing commands on the master part, it has been chosen manually. That range is selected so that its extremes are enough high for the operator to feel force changes and low enough not to move the user hand on the master or damage any of the physical protections around it.

Thus, the torque values calculated from the forces are multiplied by a gain of 100 (in addition to the gains of the system itself), and a saturation has been placed on the scheme with limits of -0.1 DSP and +0.1 DSP for protection of the device.

It should be emphasized that this adaptation is only implemented because of the lack of a proper calibration.

Another add-on to the schematic of appendix II is an initialization measure as a way of protection, so that the first 5 seconds there is no command applied to the master. This has been implemented to make sure that the transient part of the filters has finished and the signal that it is being amplified is the correct one.

4.2.3 Results

This implementation has been tested with the mock-up lung in an attempt to visualize on the signals the difference when there is soft healthy tissue of the lung and when there is a nodule. The mock-up lung has been placed between the two arms and the principal motion has been the one in compression due to the fact that it provided more information.

The results of the palpation can be seen on figure 4.10, where green areas represent contact with normal areas of the lung and red areas imply palpation of a nodule.

On the first graphs there is the position of both the master and the slave, being the master position the input and the slave one the output. Now, when there is an obstacle (being that the healthy lung or a nodule on it), there are forces applied to the master's tip in the opposite direction of the movement, so the reference has a motion constraint and it doesn't change while the response is not able to, unlike in figure 4.5. Even so, there is an increase on the error when there is contact with the environment. Table 4.3 gathers the difference between the input and the output in degrees.

	Position error (º)	
	Compression	**Shear**
No obstacle	0,05	0,08
Soft tissue	0,5	0,22
Nodule	0,9	0,25

Table 4.3: Position error between the reference and the response of both arms

The error values are consistent with the ones of previous tests when there is no interaction with the environment, where the compression arm has a smaller error than the shear arm.

However, when the palpation is happening, meaning there is contact, the compression error is higher than the shear one. That can be explained because on the compression motion, the nodule pushed by the arm finds kind of a support on the shear arm, so there is a motion constraint on that direction that affects the response more than in the shear case, where the arm has more ease to translate even when in contact with the nodule. This also explains why there is a shear force every time there is a compression force, because if the shear arm is placed just below the nodule, the compression force is transferred to the shear arm through the nodule.

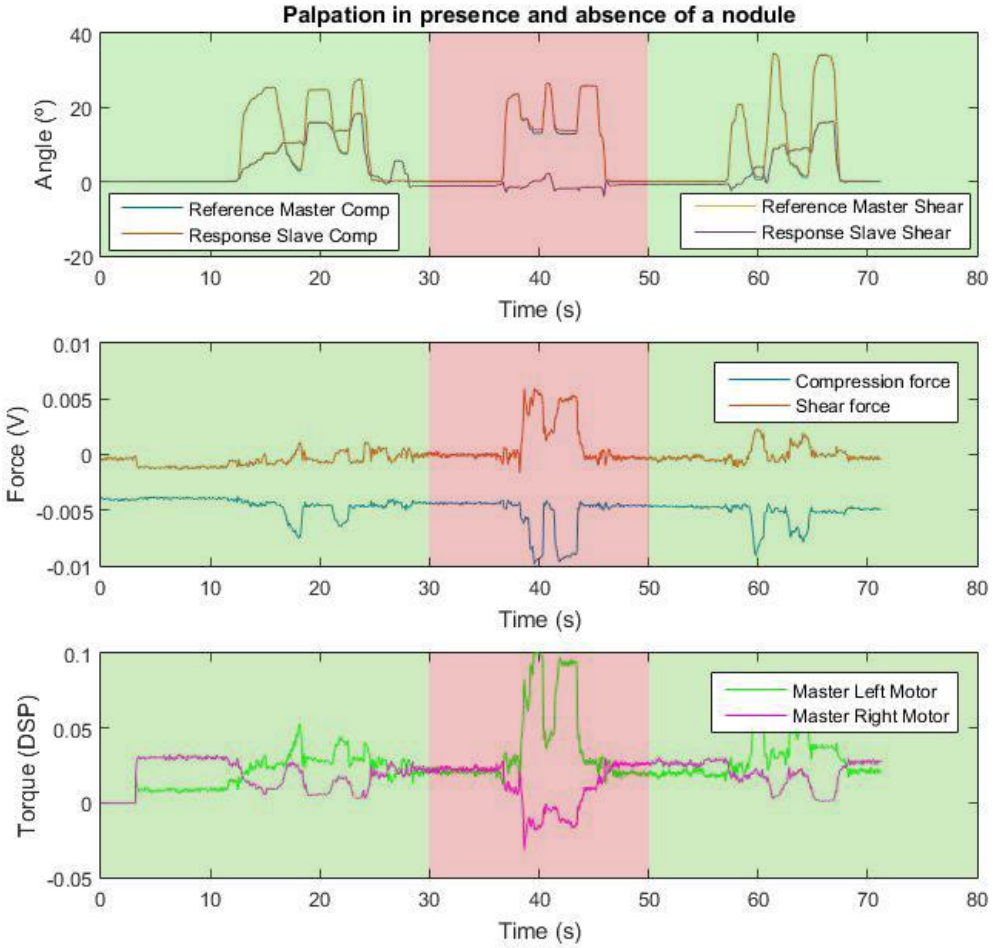

Figure 4.10: Results of a two-way teleoperation during palpation

Finally, the results show that the torques are bigger when there is a presence of a lung nodule, and the force feeling at the master during the experiment was also higher.

With the proper sensor calibration, the next step would be to use a closed-loop controller, where the force interaction between the device and the operator is compared with the one measured on the master, and the developed torques are accordingly corrected by the action of the controller.

Chapter 5

Conclusions

This thesis presents the continuation of a series of studies on a teleoperated palpation device, starting from a research and a familiarization with the device, then a more theoretical part of the project and finally an implementation, where the proposed things were put into practice.

The main objective of this project was to end up having a bilateral teleoperation, by controlling in the first place the motion of the slave and adding later a force-feedback with a force control on the master so that it can provide a haptic feeling to the operator during the lung palpation.

All the followed steps have led to reach that objective, and the defined goals of each middle step have been achieved. However, there is still plenty of room for improvement, starting by a proper calibration of the force sensors (both in the master and the slave) to be able to have the real values of the forces on the palpation task.

On the personal, this project has let me explore the whole process of working with a real device and allowed me to learn from the troubles and limitations that come with the transition from theory to practice.

To conclude, if I weigh the pros and cons of doing the master thesis in a foreign country and in a new university, the decision seems to be the right one because it has given me more opportunities of learning than the obstacles that I may have found on the way.

Appendix I

ControlDesk interface

As commented briefly on section 2.3, there is an interaction between Simulink and ControlDesk. That is done by adding the DS1103 Controller Board blocks in Simulink, which are the following:

Block	Function
« ENCODER MASTER SETUP »	Initialization of the inputs/outputs of the controller
«ENCODER SET POSITION»	Definition of the initial value of an encoder
«ENC POSITION»	Recovery of an encoder output value
«DAC»	Sending a command to a motor
«MUX_ACD»	Recovery of a force sensor output value

With the «ENCODER SET POSITION» block, all encoders are initialized at 0 having the device on the reference position, where the grasper is centered and closed, and the master centered on its rest position. This block allows to choose the corresponding channel for initializing each encoder.

The «ENC POSITION» block gives the position of the motor on the selected channel, but it needs to be converted into radians. As the encoders count 1024 pulses/rev, after all these blocks there is a gain block with a value of $2\pi/1024$ that converts the pulses into radians.

The «DAC» block send the commands on DSP units, with values that are comprised between -1 and +1, which correspond to -10V and +10V.

Finally, the «MUX_ACD» provides signals in volts that are proportional to the measured forces.

Once the desired Simulink schematic is done, a model is built in C/C++ code and a *.sdf* file is generated and used by ControlDesk to retrieve all the information on the system.

The ControlDesk software has plenty of instrumentation for updating and measuring the different variables. The main ones employed for this project are the plot tool, value indicators, the numeric input tool and sliders. The two first ones are for visualizing and collecting data whilst the two last ones allow the user to act on the variables online. Figure I.1 shows the appearance of this interface with the instrumentation.

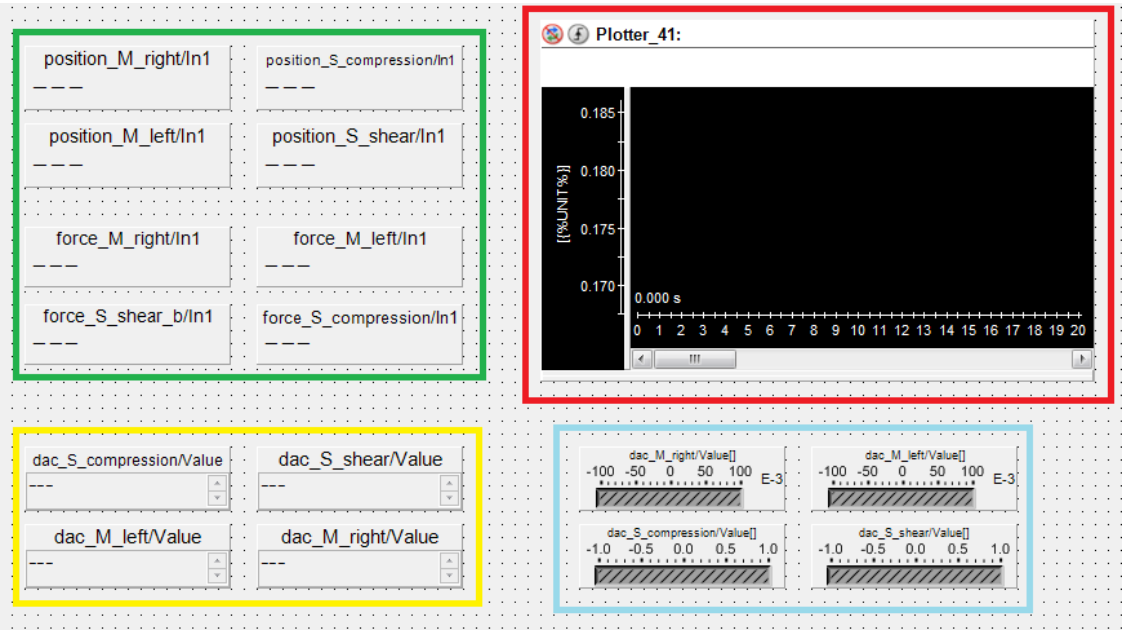

Figure I.1: ControlDesk interface. Green: Value indicators; Red: Plot tool; Yellow: Numeric inputs; Blue: Sliders.

After running an experiment, the software allows to export the collected data to Matlab format (fig. I.2), so that it can be properly processed.

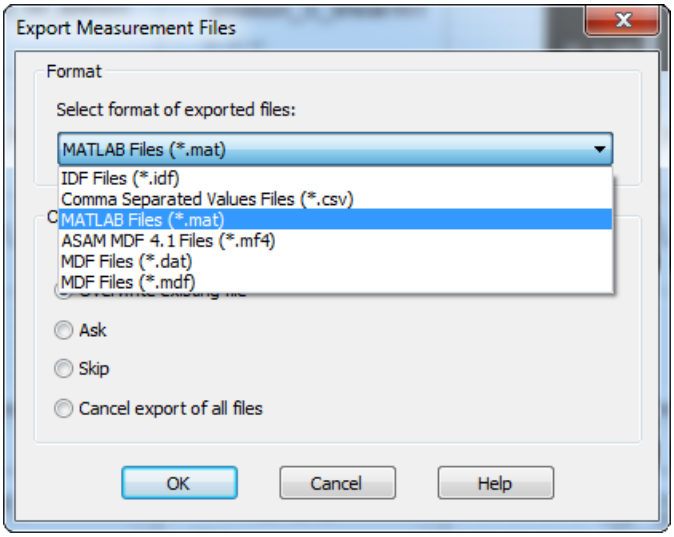

Figure I.2: Export Measurement Files window

Appendix II

Simulink schemes

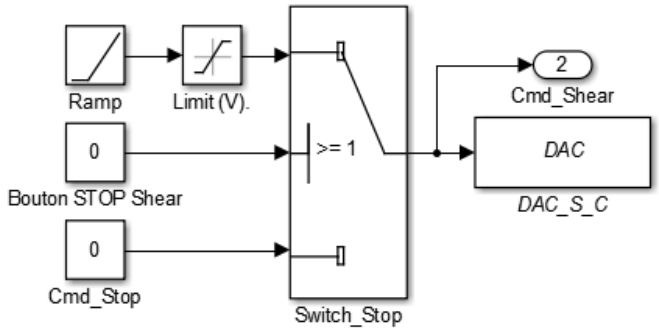

Figure II.1: Simulink schematic for applying a ramp

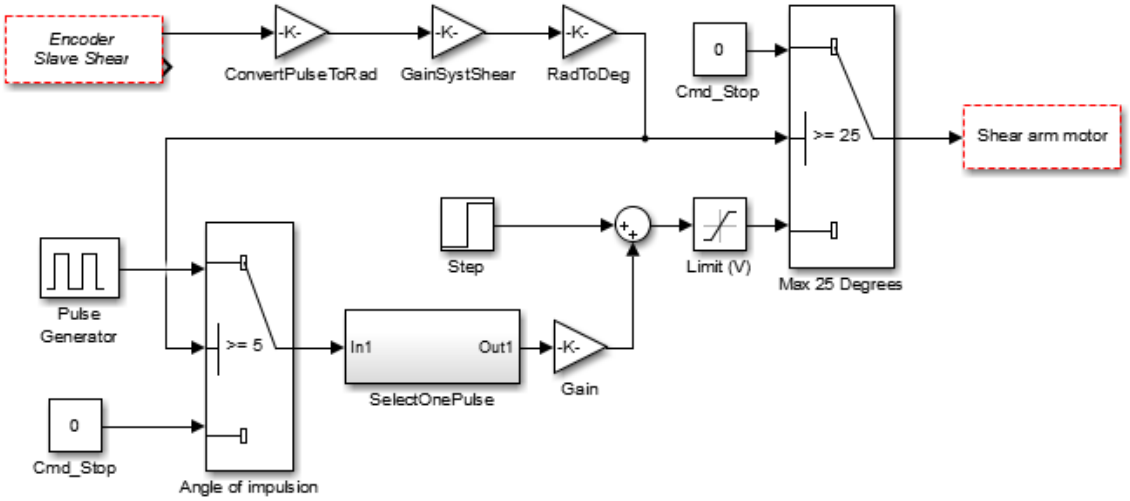

Figure II.2: Simulink schematic for applying a step and a pulse

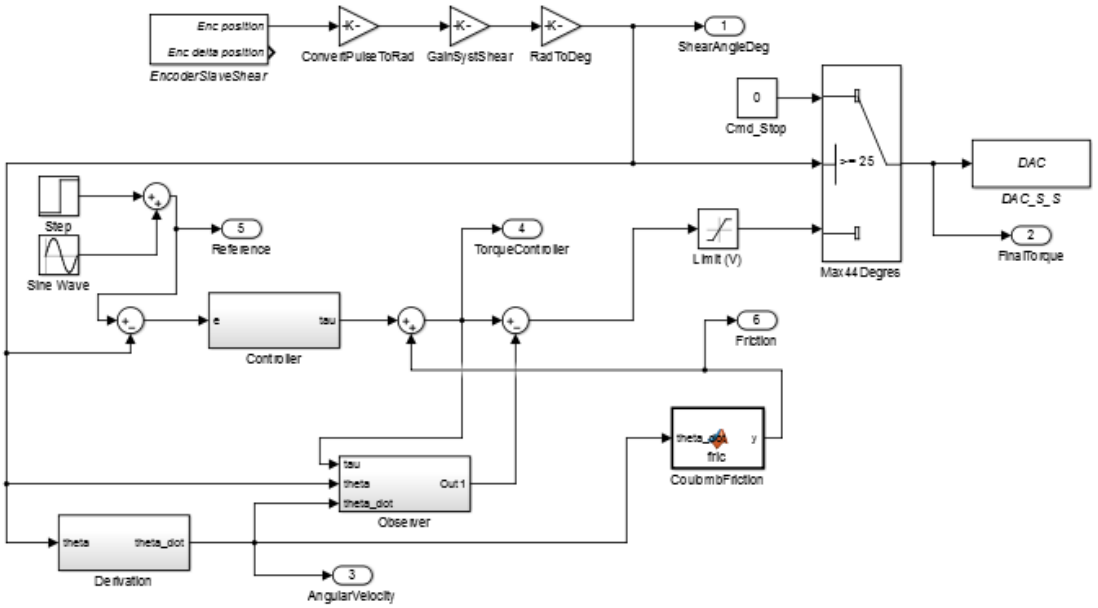

Figure II.3: Implementation of motion control of the slave

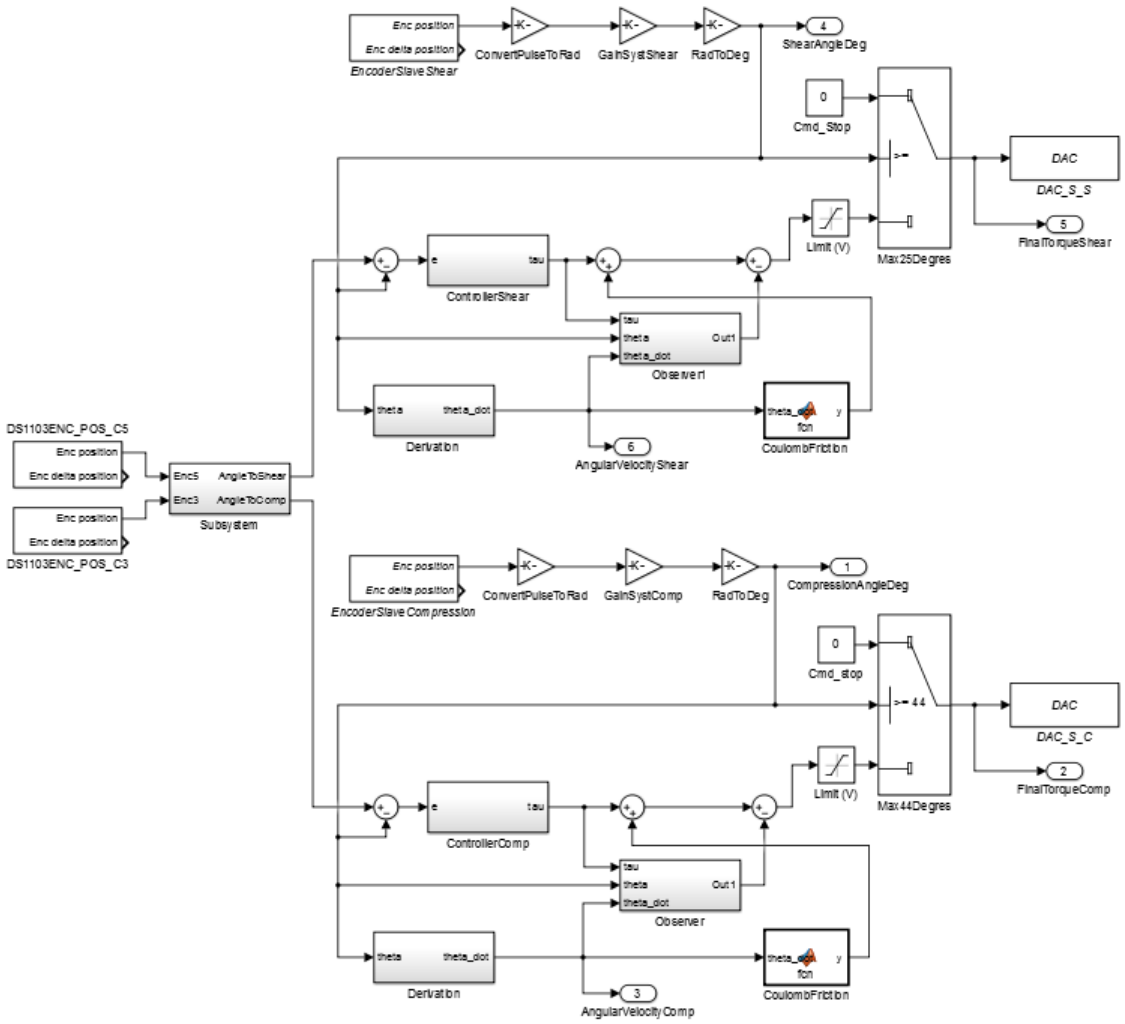

Figure II.4: Schematic for unilateral teleoperation

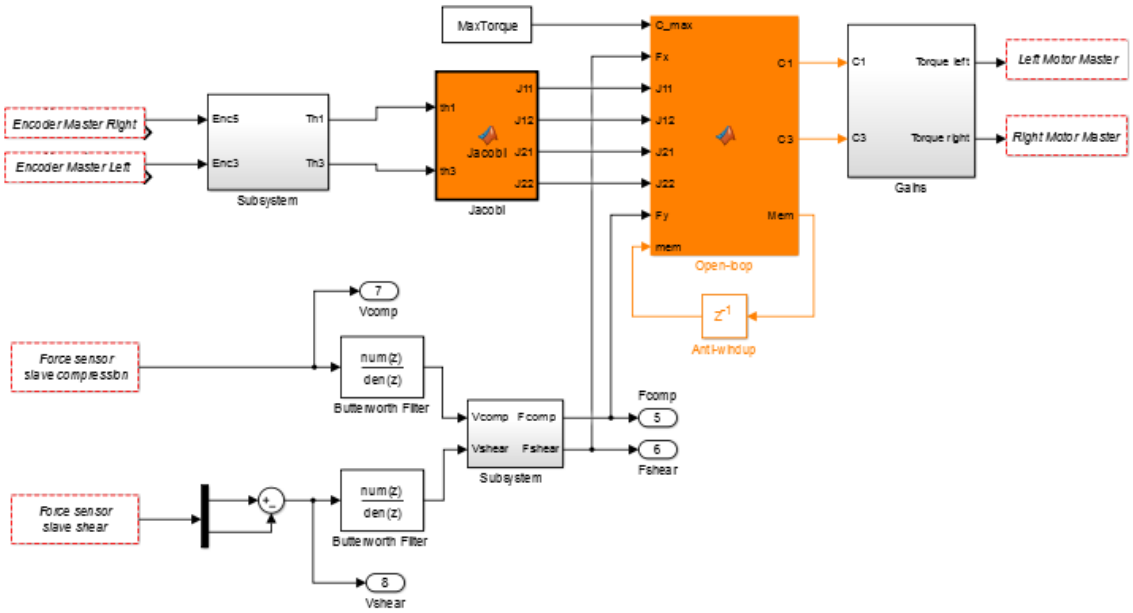

Figure II.5: Schematic for the force control part on bilateral teleoperation

References

[1] http://www.uchospitals.edu/specialties/minisurgery/benefits/

[2] A. Demira, K. Ayalpb, B. Ozkana, E. Kabab, A. Tokera. *Robotic and video-assisted thoracic surgery lung segmentectomy for malignant and benign lesions*. Interactive CardioVascular and Thoracic Surgery. 2014.

[3] http://www.davincisurgery.com/

[4] https://my.clevelandclinic.org/health/diseases_conditions/hic_Pulmonary_Nodules

[5] Cancer Research UK / Wikimedia

[6] A. Buttafuoco. *Design and Control of a Teleoperated Palpation Device for Minimally Invasive Thoracic Surgery*. PhD thesis, Ecole Polytechnique de Bruxelles, 2013.

[7] A. P. Miller, W. J. Peine, J. S. Son, Z. T. Hammoud M.D. *Tactile Imaging System for Localizing Lung Nodules during Video Assisted Thoracoscopic Surgery*. IEEE International Conference on Robotics and Automation, 2007.

[8] V. D. M. Hornblower, E. Yu, A. Fenster, J. J. Battista, R. A. Malthaner. *3D thoracoscopic ultrasound volume measurement validation in an ex vivo and in vivo porcine*. Physics in Medicine and Biology, 52(1):91, 2007.

[9] M.O. Culjat, J. W. Bisley, Chih-Hung King, C. Wottawa, R. E. Fan, E. P. Dutson, W. S. Grundfest. *Tactile Feedback in Surgical Robotics.* Surgical Robotics, Systems Applications and Visions. 2011.

[10] M. D. Naish, R. V. Patel, A. L. Trejos, M. T. Perri, R. A. Malthaner. *Robotic Techniques for Minimally Invasive Tumor Localization*. Surgical Robotics, Systems Applications and Visions. 2011.

[11] M. Cottin. *Réalisation d'un asservissement Position-Position sur un dispositif de palpation téléopéré*. Rapport de stage TECHNIQUE de 4ième année, Polytech Grenoble, 2014.

[12] D.Wiltgen. *Control of a force-feedback teleoperated palpation device for minimally invasive surgery*. Master thesis, Ecole Polytechnique de Bruxelles, 2015.

[13] MAXON Motor: http://www.maxonmotor.es/maxon/view/catalog. January 2016.

[14] Vishay Precision Group: http://www.vishaypg.com/. January 2016.

[15] dSPACE: https://www.dspace.com/home/products/hw/singbord/ppcconbo.cfm. January 2016.

[16] MATLAB R2015a, The MathWorks Inc., Natick, MA, 2015.

[17] ControlDesk 5.5, dSPACE Inc., Wixom, MI, 2015.